

Cosmological Inflation in N -Dimensional Gaussian Random Fields with Algorithmic Data Compression

Connor A. Painter and Emory F. Bunn

Physics Department, University of Richmond, Richmond, VA 23173, USA

There is considerable interest in inflationary models with multiple inflaton fields. The inflaton field ϕ that has been postulated to drive accelerating expansion in the very early universe has a corresponding potential function V , the details of which, such as the number of dimensions and shape, are free parameters of the theory. We consider a natural hypothesis that V ought to be maximally random. We realize this idea by defining V as a Gaussian random field in some number N of dimensions. Given a model set of parameters that statistically determine the shape of V , we repeatedly evolve ϕ through the end of inflation from various initial conditions, cataloguing a representative sample of trajectories associated with that model. In order to impose the anthropic constraint of a universe in which inflation ends and normal expansion takes over, we impose a minimum with $V = 0$ and only consider trajectories that reach that minimum. We simulate each path evolution stepwise through ϕ -space while simultaneously computing V and its derivatives along the path via a constrained Gaussian random process. When N is large, this method significantly reduces computational load as compared to methods which generate the potential landscape all at once. Even so, the covariance matrix Γ of constraints on V can quickly become large and cumbersome. To solve this problem, we present data compression algorithms to prioritize the necessary information already simulated, then keep an arbitrarily large portion. With these optimizations, we simulate thousands of trajectories with various parameter sets, extract tensor and scalar perturbation spectra from each, then assemble statistical predictions of these quantities through repeated trials. We find that the Gaussian random potential is a highly versatile inflationary model with a rich volume of parameter space capable of reproducing modern observations.

I. INTRODUCTION

Characterization of plausible inflationary models is an extremely high priority in cosmology [1]. Since inflationary theory was developed in the late 1970s and 80s, the cosmological community has sought to constrain the parameter space of possible inflationary models (e.g., [2]). Some parts of this parameter space – in particular, some choices for the inflaton potential V – have been explored in exhaustive detail, but the vastness of the parameter space defies complete exploration.

Potentials with a large number of inflaton degrees of freedom N [3] are potentially of particular interest. In particular, they may be a natural consequence of string theory [4]. Even if we lay string theory aside, it is extremely plausible to imagine that many additional fields may occur as we extend our model of particle physics to the vastly higher energies at which inflation is thought to have occurred. Fully exploring a theory with $N \gg 1$ inflaton fields, with an unknown potential $V(\phi^{(0)}, \dots, \phi^{(N-1)})$, is a computationally daunting task.

Rather than specifying a fixed potential *a priori*, it may be natural to consider models inspired by the “landscape” of string theory, in which V is taken to be a realization of a random process, often taken to be a Gaussian process with a Gaussian correlation function. One can imagine making predictions for this model by generating many random realizations of the potential, simulating the dynamics of the inflaton fields, and using the result to make predictions for observable quantities (scalar and tensor power spectra, non-Gaussianity, etc.) In a high-dimensional space, simulating a realization through-

out an entire box is computationally intractable. Fortunately, we need the simulation only along the inflaton path.

The most well-developed method for making predictions in such models is built on methods of random matrix theory (RMT) (e.g., [5–11] and references therein). These methods are based on approximations and assumptions that may be problematic [12–15]. Among other issues, these methods can lead to solutions that do not have continuous derivatives, which can lead to problems in making predictions of non-Gaussianity [16], although adaptations are possible [17].

Other methods besides RMT have been used to explore multifield inflation in random potentials. Some involve simulating the potential in the vicinity of a single point [15, 16]. Other methods involve random walks [18], Bayesian networks [19], and machine learning [20].

In this paper, we present a method of simulating trajectories in a random landscape directly, without recourse to the approximations involved in techniques such as RMT. At each step along the numerical solution of the inflaton equations of motion, we simulate the potential, taking into account the information provided by the simulations at previous steps along the path. (Similar methods are found in [21].) In order to keep the computation from becoming intractable, we periodically “forget” information that no longer significantly influences the simulation.

The paper is structured as follows: requisite multifield inflationary theory is presented in the remainder of Section I, the generation of Gaussian random potentials is formalized in Section II, our original code and data

compression algorithms are detailed in Section III, results are given in Section IV, and we conclude with Section V.

A. Multi-field Inflation

As customary in inflationary theory, we suppose there existed some “inflaton” field $\phi(t, \mathbf{x})$ which permeated the early universe with time evolution governed by its associated potential function $V(\phi)$. We assume that the inflaton field was spatially homogeneous with small perturbations, i.e., $\phi(t, \mathbf{x}) \approx \phi(t) + \delta\phi(t, \mathbf{x})$. In general, $\phi = (\phi^{(0)}, \phi^{(1)}, \dots, \phi^{(N-1)})$ is a vector of N components while V is scalar-valued. In addition to its existence, we assert that the inflaton potential dominates the energy density of the early universe so that its characteristics may determine the particularities of large-scale cosmic expansion in early times. The Klein-Gordon equation for the evolution of ϕ is

$$\ddot{\phi} + 3H\dot{\phi} + \nabla_\phi V = 0, \quad (1.1)$$

where overdots signify derivatives with respect to cosmic time t , H is the Hubble parameter, and Planck units $c = \hbar = 8\pi G = 1$ are implemented throughout. Equation (1.1) is written componentwise as

$$\ddot{\phi}^{(\alpha)} + 3H\dot{\phi}^{(\alpha)} + \frac{\partial V}{\partial\phi^{(\alpha)}} = 0, \quad (1.2)$$

for $\alpha = 0, \dots, N-1$. As is well known, this system of equations is equivalent to a ball rolling in the potential V with a friction force given by the Hubble parameter.

The Hubble parameter is related to the field by the Friedmann equation,

$$3H^2 = \frac{1}{2}|\dot{\phi}|^2 + V. \quad (1.3)$$

Given the potential, the second-order differential equation (1.2) can be solved numerically with initial conditions $\phi_i = \phi(t_i)$ and $\dot{\phi}_i = \dot{\phi}(t_i)$. Often, the initial rate of change is set to slow-roll equilibrium so that $\ddot{\phi}_i = 0$. By (1.1), the approximation is

$$\dot{\phi}_i \approx -\frac{\nabla_\phi V_i}{3H_i}. \quad (1.4)$$

Furthermore, if $|\dot{\phi}|^2$ is assumed to be negligibly small, then (1.3) reduces to $3H^2 \approx V$ and the slow-roll approximation is

$$\frac{\dot{\phi}_i}{H_i} \approx -\frac{\nabla_\phi V_i}{V_i}. \quad (1.5)$$

For numerical and analytic purposes, it is often useful to measure time in terms of the expansion of the universe [22]. During inflation, the scale factor $a(t)$ grows approximately exponentially, so a natural unit of time is the “number of e -folds”

$$N_e(t) = \ln\left(\frac{a(t)}{a(t_i)}\right), \quad (1.6)$$

where t_i is some arbitrary start time of inflation. Since $H = \dot{a}/a$, the left-hand side of (1.5) then simplifies to $d\phi_i/dN_e$ and, under slow roll, some algebra transforms (1.2) into

$$\frac{d^2\phi^{(\alpha)}}{dN_e^2} + (3-\epsilon)\frac{d\phi^{(\alpha)}}{dN_e} + \frac{1}{H^2}\frac{\partial V}{\partial\phi^{(\alpha)}} = 0, \quad (1.7)$$

in which we have defined the slow-roll parameter ϵ as

$$\epsilon \equiv -\frac{\dot{H}}{H^2} = \frac{1}{2}\left|\frac{d\phi}{dN_e}\right|^2, \quad (1.8)$$

signaling the end of inflation at t_e when $\epsilon \uparrow 1$. Note that H can be computed at any time step by

$$H^2 = \frac{V}{3-\epsilon}. \quad (1.9)$$

Once numerical integration finishes at $\epsilon = 1$, the values of ϕ , $\dot{\phi}$, V , $\nabla_\phi V$, ϵ , and H are known at discrete times between t_i and t_e . We refer to this set of information as the inflaton field *trajectory*.

B. Power Spectra

Various observable quantities can be extracted from the trajectory, such as the power spectra of adiabatic curvature (matter) fluctuations \mathcal{P}_S and tensor fluctuations \mathcal{P}_T , and the non-Gaussianity of the CMB [19]. In this paper, we will focus on the power spectra.

Following [22], matter perturbations evolve with the mode matrix ψ , an expansion of the comoving fluctuations $\delta\phi$ in the inflaton field. For any given mode k , the mode matrix obeys

$$\frac{d^2\psi}{dN_e^2} + (1-\epsilon)\frac{d\psi}{dN_e} + \left(\frac{k^2}{a^2H^2} - 2 + \epsilon\right)\psi + \mathbf{C}\psi = 0, \quad (1.10)$$

where the coupling matrix \mathbf{C} is defined as

$$\begin{aligned} \mathbf{C}^{(\alpha\beta)} &= \frac{1}{H^2}\left(\frac{d\phi^{(\alpha)}}{dN_e}\frac{\partial V}{\partial\phi^{(\beta)}} + \frac{d\phi^{(\beta)}}{dN_e}\frac{\partial V}{\partial\phi^{(\alpha)}} + \frac{\partial^2 V}{\partial\phi^{(\alpha)}\partial\phi^{(\beta)}}\right) \\ &\quad + (3-\epsilon)\frac{d\phi^{(\alpha)}}{dN_e}\frac{d\phi^{(\beta)}}{dN_e}. \end{aligned} \quad (1.11)$$

Given conditions on ψ and $d\psi/dN_e$ at t_i , equation (1.10) can be solved numerically up through t_e . At any given time, $\mathcal{P}_S(k)$ is computed as

$$\mathcal{P}_S(k) = \frac{k^3}{4\pi^2\epsilon}\frac{1}{a^2}\Psi\Psi^*, \quad (1.12)$$

where $\Psi = \dot{\phi} \cdot \psi/|\dot{\phi}|$, and $*$ is the conjugate transpose. To be clear, the power spectrum, as with the mode matrix, is a function of both wavenumber and time. We are interested in the shape of $\mathcal{P}_S(k)$ at the end of inflation, as this spectrum will most closely resemble modern

Quantity	Constraint
$\log(10^{10} A_S)$	3.040 ± 0.016
n_S	0.9626 ± 0.0057
$r(k_t)$	< 0.1

TABLE I. Planck constraints on matter and tensor fluctuations [23].

observed data. At t_e , we expect it to resemble a power law of amplitude A_S and index n_S around the pivot scale $k_0 = 0.05 \text{ Mpc}^{-1}$:

$$\mathcal{P}_S(k) \Big|_{t_e} \approx A_S \left(\frac{k}{k_0} \right)^{n_S - 1}. \quad (1.13)$$

For any reasonable inflationary model, \mathcal{P}_S can be evolved through time at several modes evenly log-spaced around k_0 via (1.10), then fit to (1.13) at t_e . The best fit parameters A_S and n_S can then be used to gauge the viability and predictive power of the choice of inflaton potential and initial conditions.

Following [2], the power spectrum of tensor perturbations is surprisingly easy to compute:

$$\mathcal{P}_T(k) = \frac{2}{\pi^2} H(t(k))^2. \quad (1.14)$$

The one-to-one and onto function $t(k)$ yields the time at which a scale of magnitude k last exited the horizon, most easily expressed as its inverse, $k(t) = a(t)H(t)$. Thus, in this definition, $\mathcal{P}_T(k)$ gives by default the power at the end of inflation. As with the matter spectrum, the tensor spectrum can be sampled at several wavenumbers around k_0 and fit to another anticipated power law,

$$\mathcal{P}_T(k) \approx A_T \left(\frac{k}{k_0} \right)^{n_T}. \quad (1.15)$$

The tensor perturbation amplitude is often expressed in terms of the tensor-to-scalar ratio r , which is defined as the power law ratio for any given k ,

$$r(k) = \frac{\mathcal{P}_T(k)}{\mathcal{P}_S(k)} = \frac{A_T}{A_S} \cdot \left(\frac{k}{k_0} \right)^{n_T - n_S + 1}. \quad (1.16)$$

We will quote tensor-to-scalar ratios at the scale $k_t = 0.002 \text{ Mpc}^{-1}$.

Constraints on A_S , n_S , and $r(k_t)$ have been found by recent Planck missions and are summarized in Table I [23].

II. FORMALISM

The review in Section I was independent of the inflaton potential, but a specification of $V(\phi)$ is the heart of every inflationary model. In this paper, we assume that $V(\phi)$ is a realization of an N -dimensional Gaussian random field with mean zero, coherence scale s , and energy

scale V_\star [18]. The coherence scale s is the distance in ϕ -space below which values of V are strongly correlated. To be specific, the potentials at all points are drawn from a multivariate normal distribution with mean zero and covariance

$$\langle V(\phi_i)V(\phi_j) \rangle = V_*^2 \exp \left(-\frac{|\phi_i - \phi_j|^2}{2s^2} \right), \quad (2.1)$$

so points separated by a distance s have correlation $e^{-1/2} \approx 0.6$. Random potentials with high s are “stretched” horizontally, take longer to evolve, and accrue more e -folds of inflation.

The inflationary energy scale V_\star is the standard deviation of V . In order to produce scalar fluctuations at levels that approximately match observations, V_* should be of order $10^{-5} E_{\text{Pl}}^4$.

A. Generating Correlated Points

In order to simulate a trajectory, one could begin by simulating the potential V throughout an N -dimensional box in which the trajectory is expected to lie, but for large N this is extremely inefficient. It is far preferable to generate V along with the trajectory, determining its value at each new point on the trajectory only when we need it. We describe and implement this method of simulating V along the path of ϕ in the following sections.

Generating points on a Gaussian random field is a constrained random process; every new point is generated randomly *constrained by* every previously generated point. This is necessary to ensure that the potential has the desired correlation structure – in particular, that it is appropriately smooth on scales less than s .

Suppose that V is known at sequence of o points $\phi_0, \phi_1, \dots, \phi_{o-1}$, and group those values in a vector $\mathbf{v}_{\mathcal{O}}$. Now, we want to know V at n new points $\phi_o, \phi_{o+1}, \dots, \phi_{o+n-1}$, and we call those unknown values $\mathbf{v}_{\mathcal{N}}$. First, we need to define the *covariance matrix* Γ of constraints on V as an $(o+n) \times (o+n)$ matrix with elements

$$\Gamma^{(ij)} = \langle V(\phi_i)V(\phi_j) \rangle \equiv \langle V_i V_j \rangle, \quad (2.2)$$

where the covariances are given by equation (2.1).

This symmetric, positive-definite matrix is then broken up into blocks corresponding to the type of information stored,

$$\Gamma = \begin{bmatrix} \Gamma_{\mathcal{O}\mathcal{O}} & \Gamma_{\mathcal{O}\mathcal{N}} \\ \Gamma_{\mathcal{N}\mathcal{O}} & \Gamma_{\mathcal{N}\mathcal{N}} \end{bmatrix}, \quad (2.3)$$

where \mathcal{O} abbreviates “old” data and \mathcal{N} abbreviates “new” data [24], so $\Gamma_{\mathcal{O}\mathcal{O}}$ contains covariances of old points, $\Gamma_{\mathcal{O}\mathcal{N}} = \Gamma_{\mathcal{N}\mathcal{O}}^T$ contains cross-covariances between old and new points, and $\Gamma_{\mathcal{N}\mathcal{N}}$ contains covariances of new points. Since covariances are functions of known

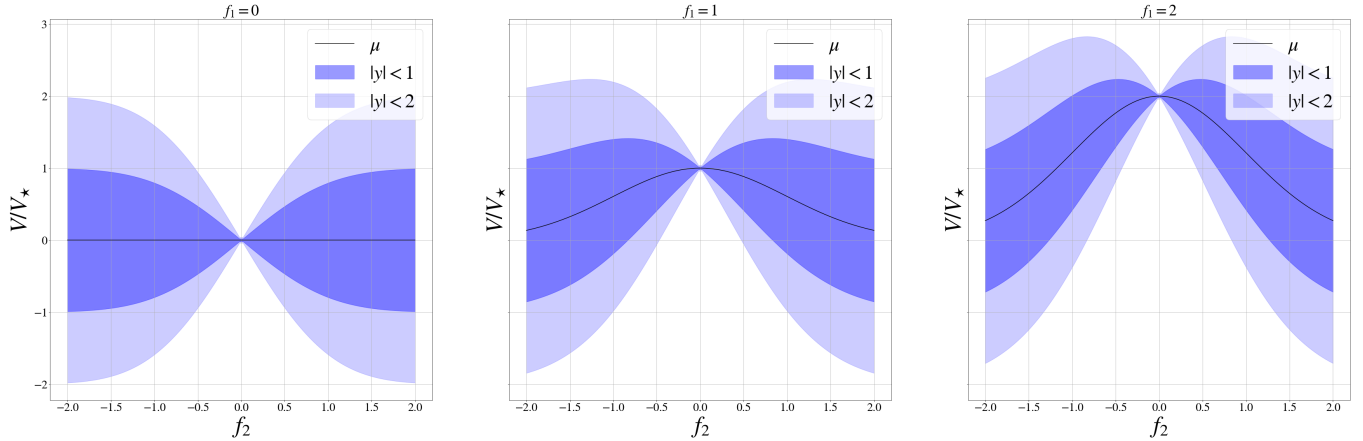


FIG. 1. One-two sigma contour plots of the correlation between two points as a function of their separation in a Gaussian random process. Given $V(\phi_0) = f_1 V_*$ and simulating $V(\phi_1)$ at some $|\phi_0 - \phi_1| = f_2 s$, the figure shows μ (black line) and the normal distributions for possible variation about μ . When $|f_2|$ is small, the points are close together and V will be highly constrained around $V(\phi_0)$. The influence of V_0 on V_1 decays rapidly as $|f_2|$ grows.

distances between points, Γ can be populated and used to randomly generate $\mathbf{v}_{\mathcal{N}}$.

The vector $\mathbf{v}_{\mathcal{N}}$ is drawn from the conditional probability distribution given by the multivariate normal distribution with covariance (2.3), subject to the constraints that the values of $\mathbf{v}_{\mathcal{O}}$ are known. This is a Gaussian distribution [25, 26] with mean

$$\boldsymbol{\mu} = \boldsymbol{\Gamma}_{\mathcal{N}\mathcal{O}} \boldsymbol{\Gamma}_{\mathcal{O}\mathcal{O}}^{-1} \mathbf{v}_{\mathcal{O}} \quad (2.4)$$

and covariance matrix

$$\boldsymbol{\Gamma}_{\mathcal{C}} = \boldsymbol{\Gamma}_{\mathcal{N}\mathcal{N}} - \boldsymbol{\Gamma}_{\mathcal{N}\mathcal{O}} \boldsymbol{\Gamma}_{\mathcal{O}\mathcal{O}}^{-1} \boldsymbol{\Gamma}_{\mathcal{O}\mathcal{N}}. \quad (2.5)$$

Explicitly,

$$\mathbf{v}_{\mathcal{N}} = \boldsymbol{\mu} + \boldsymbol{\sigma}. \quad (2.6)$$

Here

$$\boldsymbol{\sigma} = \boldsymbol{L}_{\mathcal{C}} \mathbf{y}, \quad (2.7)$$

where $\boldsymbol{\Gamma}_{\mathcal{C}} = \boldsymbol{L}_{\mathcal{C}} \boldsymbol{L}_{\mathcal{C}}^T$ is the lower-triangular Cholesky decomposition and \mathbf{y} is a vector of n independent standard normal values drawn from $\mathcal{N}(\mathbf{0}, \mathbf{1})$.

As a simple example, suppose we sample $V(\phi_0)$ to be $f_1 V_*$ and I seek to generate $V(\phi_1)$ in which $|\phi_0 - \phi_1| = f_2 s$. In this case, the covariance matrix is

$$\boldsymbol{\Gamma} = \begin{bmatrix} V_*^2 & V_*^2 \exp(-f_2^2/2) \\ V_*^2 \exp(-f_2^2/2) & V_*^2 \end{bmatrix}. \quad (2.8)$$

Since $n = 1$, the mean is a scalar,

$$\mu = f_1 V_* \exp\left(-\frac{f_2^2}{2}\right), \quad (2.9)$$

as is the conditional covariance matrix,

$$\boldsymbol{\Gamma}_{\mathcal{C}} = V_*^2 [1 - \exp(-f_2^2)]. \quad (2.10)$$

Some one-two sigma contour plots of possible generations of $V(\phi_1)$ are presented in Figure 1. Note that as $|f_2|$ grows, μ trends from $V(\phi_0)$ toward zero, the unconstrained mean, and σ moves from zero toward yV_* , another appropriate trend since without constraints $\langle \sigma^2 \rangle = V_*^2 \langle y^2 \rangle = V_*^2$. In other words, the value of V_1 is highly constrained around V_0 when ϕ_1 is close to ϕ_0 , and the constraints weaken as the separation grows.

Constrained random generation of potential information is not restricted to values of V ; the covariance matrix $\boldsymbol{\Gamma}$ can handle any ϕ -derivatives as well. For example, if one element $v^{(i)}$ of \mathbf{v} is a value of $\partial V / \partial \phi^{(\alpha)}$, and another element $v^{(j)}$ is a value of V , then

$$\Gamma^{(ij)} = \left\langle \frac{\partial V_i}{\partial \phi_j^{(\alpha)}} V_j \right\rangle = \frac{\partial}{\partial \phi_j^{(\alpha)}} \langle V_i V_j \rangle \quad (2.11)$$

$$= \left(\frac{\phi_j^{(\alpha)} - \phi_i^\alpha}{s^2} \right) \langle V_i V_j \rangle \quad (2.12)$$

All correlations between first and second derivatives of V follow from this method, albeit with tedious algebra.

B. The Minimum Condition

Generic inflaton trajectories do not lead to universes like our own: the solution settles into a minimum of V that is generically quite far from zero, leading to a universe that either inflates forever or rapidly recollapses. When comparing with observation, we wish to look at models that are anthropically constrained (e.g., [27–29]) to end in a minimum whose value is extremely close to zero.

We implement this anthropic constraint by imposing the following $N^2 + N + 1$ conditions on V before the

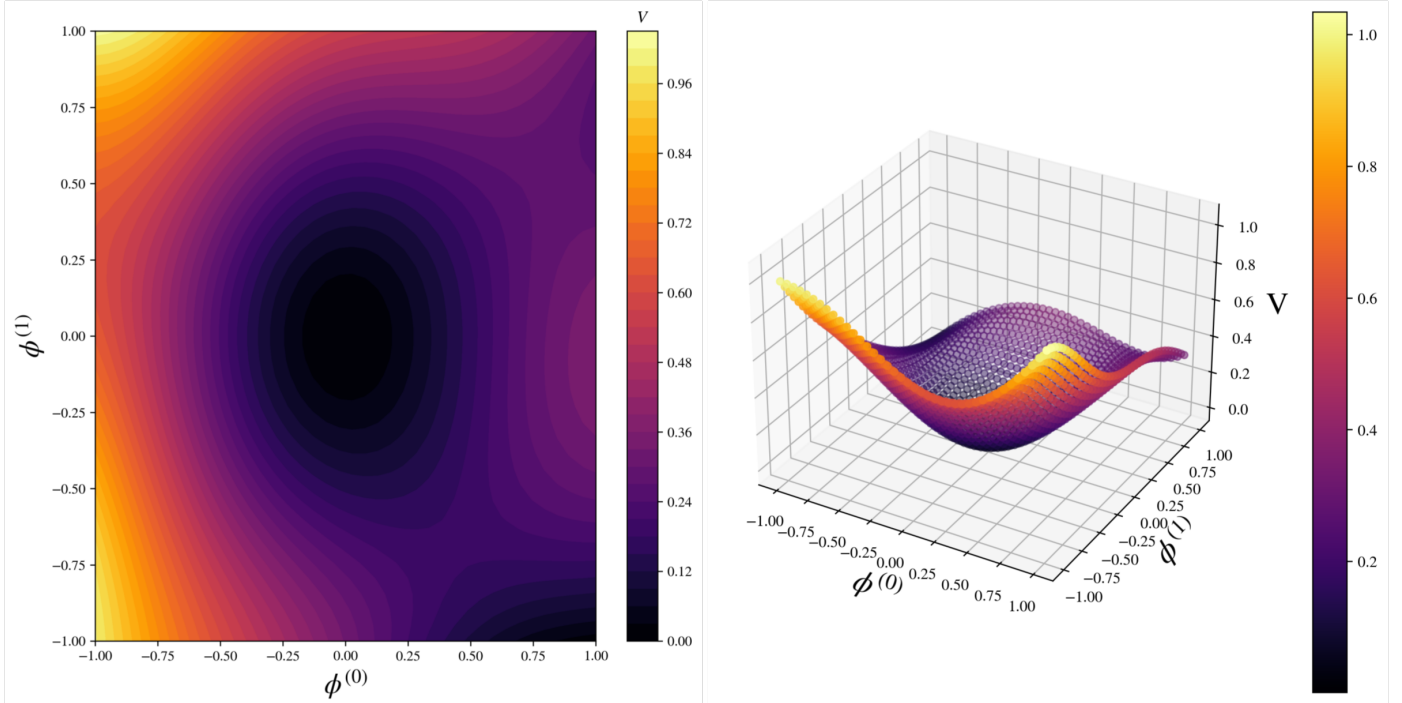


FIG. 2. A 2-dimensional Gaussian random potential V generated at nodes on a 40×40 grid evenly spaced in $\phi^{(0)}, \phi^{(1)}$. *Left:* a “birds-eye view” of the potential isocontours, colored by potential value. *Right:* the same potential function as a traditional 3-D projection, with V as the height. In both panels, the imposed minimum conditions are clearly visible. Note that we do not employ these techniques of generating potential values throughout an entire rectangular domain when solving the trajectory, but do so here for illustrative purposes.

trajectory is solved:

$$V(\mathbf{0}) = 0 \quad (2.13)$$

$$\frac{\partial V}{\partial \phi^{(\alpha)}}(\mathbf{0}) = 0 \text{ for all } \alpha \quad (2.14)$$

$$\frac{\partial^2 V}{\partial (\phi^{(\alpha)})^2}(\mathbf{0}) > 0 \text{ for all } \alpha \quad (2.15)$$

$$\frac{\partial^2 V}{\partial \phi^{(\alpha)} \partial \phi^{(\beta)}}(\mathbf{0}) = 0 \text{ for all } \alpha \neq \beta \quad (2.16)$$

These conditions ensure that the potential is zero, flat, and concave up at the origin. More precisely, we want the Hessian \mathbf{H} to be positive-definite at the origin. Since there are no preferable locations in a Gaussian random field, we could have chosen any location for the minimum, but chose the origin for convenience. Constraints (2.15) and (2.16) are equivalent to diagonalizing \mathbf{H} and forcing its diagonal elements to be positive. Physically, we reorient our axes to align with the principal directions of curvature. This is a surefire method of enforcing that simulations with ϕ_i in the neighborhood of the origin evolve a physically interesting path. An example potential generated with the minimum conditions is visualized in Figure 2.

III. COMPUTATIONAL PROCESS

We developed the `bushwhack` code to solve the equations of motion for the inflaton field in an N -dimensional Gaussian random potential. Careful measures were implemented to simplify and compress data related to the random generation of V , the most computationally intensive feature, in hopes of achieving simulations with higher N .

A. The Program

Figure 3 shows the general progression of the `bushwhack` program, from the input of initial conditions to the output information about predicted observable quantities. We detail each step below.

Supply initial conditions. The first step is to fix the parameters s , V_* , and N of the potential, and the initial conditions required for solving the differential equations (1.7). Since the $V = 0$ minimum will be seeded at the origin $\phi = \mathbf{0}$, and since we expect the field to evolve toward those values, it is only necessary to supply $\phi_i \equiv |\phi_i|$ instead of N vector components. Once ϕ_i is given, ϕ_i is randomized in the N -dimensional shell of that radius. This randomization is necessary to collect a representative sample of trajectories for potentials with

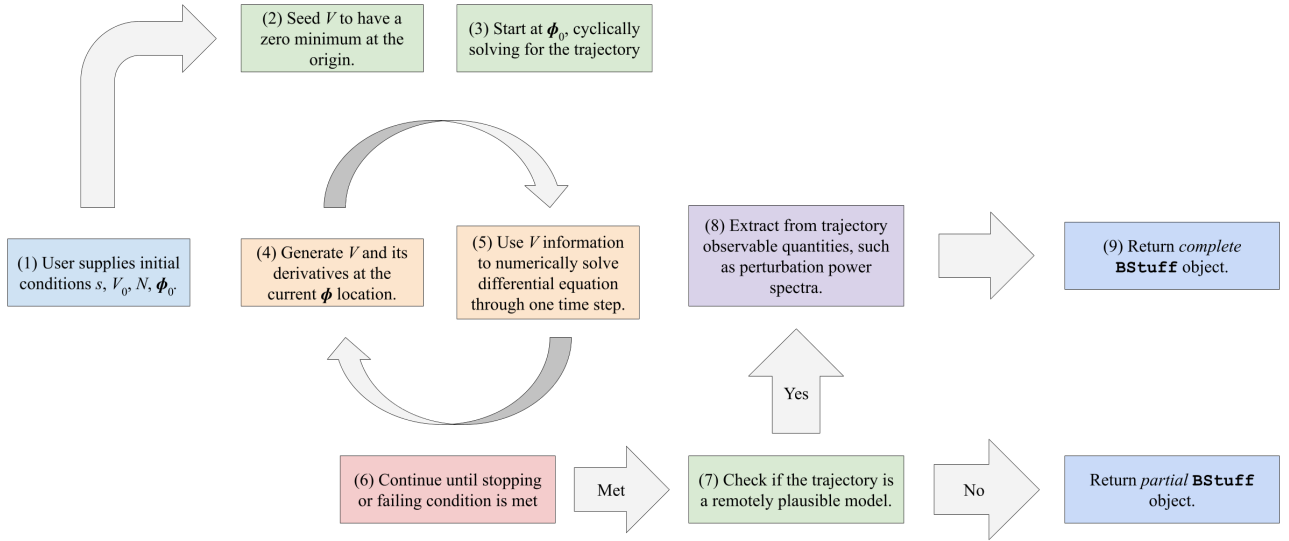


FIG. 3. Flowchart for **bushwhack** code illustrating the chronology of the computational process involved in solving for the trajectory and extracting observable quantities.

a given parameter set; forcing $\phi_i = (\phi_i, 0, 0, \dots, 0)$, for instance, would yield paths which always start along a principal axis of curvature given our method for seeding minima in Section II B. Recall that $\dot{\phi}$ need not be supplied, since its value will be automatically determined by V_i and $\nabla_\phi V_i$ via equation (1.5).

Seed the minimum. Before solving for a trajectory, the code enforces conditions (2.13)-(2.16) to ensure subsequent potential generation yields physically plausible solutions. In particular, condition (2.15) is imposed by randomly simulating N independent second derivative values, taking their absolute values to force them positive, and storing them as the diagonals of the Hessian of V at the origin. At this step, many arrays are initialized such as Γ , \mathbf{v} , ϕ , and $d\phi/dN_e$. The imposed constraints at the origin will remain the first $N^2 + N + 1$ elements of \mathbf{v} throughout the simulation and constrain the rest of the potential via a corresponding upper-left block of $\Gamma = \langle \mathbf{v} \mathbf{v}^T \rangle$.

Simulate-solve cycle. Beginning at ϕ_i , $N + 1$ data points are randomly generated, V_i and $\nabla_\phi V_i$. Those values are then substituted in equation (1.7) and the field is solved numerically through one time step to ϕ_{i+1} via a fourth-order Runge-Kutta solution algorithm. Then V_{i+1} and $\nabla_\phi V_{i+1}$ are generated and so continues the “simulate–solve cycle”. At any given time step, the potential is generated exactly along the path evolution of ϕ , constrained by all previously generated data stored in Γ . In the language of Section II A, old constraints produce $\Gamma_{\phi\phi}$, which can get very large as the simulation goes on, while $\Gamma_{\mathcal{N}\mathcal{N}}$ remains an $(N + 1) \times (N + 1)$ square repre-

senting new potential and gradient values at the current position.

The most computationally expensive steps in this cycle are those involving $\Gamma_{\phi\phi}^{-1}$ [equations (2.4) and (2.5)]. Because this matrix is symmetric positive definite, these are done via Cholesky decomposition. This decomposition can be updated incrementally to account for the new rows and columns added in each time step; it does not have to be done from scratch.

It is also worth noting that this matrix has a large condition number: many of the constraints are nearly redundant, leading to nearly null eigenvectors. To ensure numerical stability, one can add a small multiple of the identity to the matrix.

Stopping conditions. Multiple stopping conditions are monitored at every time step to supervise the evolution of ϕ . The first slow-roll parameter, ϵ , turns out to be an excellent indicator of the end of inflation. $\epsilon(t_i)$ is a small fraction of unity, but $\epsilon \uparrow 1$ as ϕ accelerates into the minimum at the origin. Additionally, we define the “inwardness” parameter ι as the alignment between the slopes of V and the minimum at any given location, or

$$\iota(\phi) \equiv (\hat{\nabla}_\phi V) \cdot \hat{\phi}. \quad (3.1)$$

where hats represent unit vectors. If $\iota < 0$ at any point during the simulation, then V is sloping away from the origin and it is extremely unlikely that ϕ will converge to the $V = 0$ minimum. As a last resort, V itself is monitored. If $V < 0$ at any point, then ϕ is in the process of converging to a negative (and, therefore, unphysical) minimum away from the origin. All three conditions —

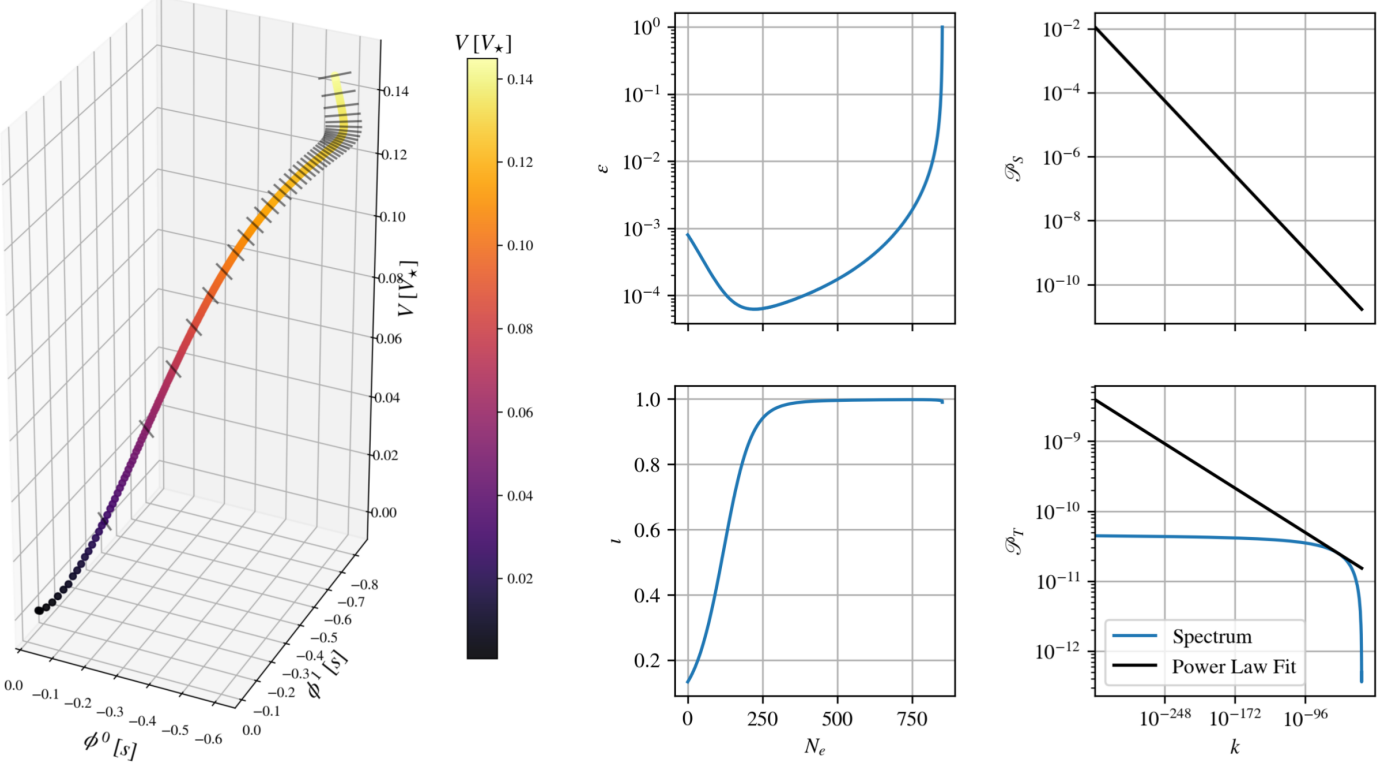


FIG. 4. A sample trajectory in a randomly generated $N = 2$ dimensional Gaussian random field with coherence scale $s = 30$ and energy scale $V_* = 5 \cdot 10^{-9}$ and some extracted observable quantities. *Left:* discrete points of the path evolution of ϕ from some initial $\phi(t_i) = s$ to the end of inflation. The potential value at each point in the evolution is represented on the vertical axis and colored. A line perpendicular to $\nabla_\phi V$ is drawn through every twentieth point. Notice how ϕ settles to the minimum seeded at the origin in late times, as desired. *Right:* the left column plots two stopping parameters as a function of number of e-folds. Notice how ϵ accelerates to 1, immediately halting integration. The inwardness parameter ι is never triggered because it never dips below zero. The right column plots two power-law fits to matter (top) and tensor (bottom) power spectra. $\mathcal{P}_S(k)$ does not have an analytic form, so only the fit is shown, while both the analytic form and the fit of $\mathcal{P}_T(k)$ are shown. Note that the approximation is only valid in the neighborhood of $k_0 = 0.05 \text{ Mpc}^{-1} \approx 1.31 \cdot 10^{-58} l_{Pl}^{-1}$.

$\epsilon \uparrow 1$, $\iota \downarrow 0$, and $V \downarrow 0$ — serve to halt the simulate-solve cycle at the precise moment when either inflation ends or the evolution goes awry. The accumulated data is then bunched into an object of original class `BStuff` and analyzed. `BStuff` objects have attributes that detail information about the field, the potential, constraints, inflation, and stopping conditions at every location along the trajectory.

Plausibility check. Once the equations of motion are solved, `bushwhack` makes an effort to determine whether the solution is a remotely plausible representative of our own universe. The verifying questions that the code asks are as follows:

1. Did the solution fail by diverging? In other words, was $\iota(\phi) < 0$ at any point? If so, do not analyze further. If not, proceed to the next check.
2. Did the solution fail by submerging? In other words, was $V(\phi) < 0$ at any point? If so, do not analyze further. If not, proceed to the next check.
3. Did the solution accumulate enough inflation? In

other words, was $N_e(t_e) \geq 55$? If so, this solution is plausible enough and observable quantities can be extracted. If not, do not analyze further.

Even if the solution fails a plausibility check, the available information is bunched and outputted as an partial `BStuff` object for further manual analysis.

Extract observables. If a trajectory is found to converge to the origin with enough inflation, observable quantities A_S , n_S , A_T , n_T , and r are extracted via methods detailed in Section 1B. To sample the matter power spectrum, note from (1.11) that it is now required to know the second derivatives of V along the path, so those are simulated sparsely along the path using Γ . It is worth emphasizing here that even with the same set of potential parameters and initial conditions on the trajectory, infinitely many random potentials and trajectories are possible, each of which yield different power spectra. It is only through repeated trials that we compile the *statistical* predictions of observable quantities from a certain parameter set. Visuals of some of the many quantities related to the trajectory and extracted observables are

presented in Figure 4.

B. Algorithmic Data Compression

Even when V is simulated only at points along the path evolution of ϕ , the covariance matrix Γ can become large and ill-conditioned. Since we add $N + 1$ additional constraints with each time step, the matrix Γ after T time steps has dimension of order $(N+1)T \times (N+1)T$ after T time steps (neglecting the additional constraints imposed to establish the minimum at the origin). With each additional time step, the number of new entries to be added is $(N+1)^2(T+1)^2 - (N+1)^2T^2 = (N+1)^2(2T+1)$. Not only must the matrix be populated, operations must be performed on it, such as Cholesky decompositions. With thousands of time steps in a typical simulation, achieving a representative sample of solutions with high N without compression methods is computationally difficult. We present two methods of data compression that can be applied iteratively throughout a simulation to limit the size of Γ while maintaining reasonable levels of accuracy in predictions of spectral quantities.

1. “Unprincipled” Forgetting

The trajectory of ϕ evolves smoothly down the slopes of V ; at some time step T , the values nearest ϕ_T are usually ϕ_{T-1}, ϕ_{T-2} , etc. By Equation (2.1), V_T and its derivatives are thus most highly constrained by V_{T-1}, V_{T-2} , etc., and their derivatives. Similarly, if $T \gg 0$, then V_T is unlikely to be highly constrained by early data. It is worth asking: how much of the information contained in Γ contributes a non-negligible constraint on new data? It is possible that early, weak constraints can be deleted while retaining the recent, relevant core of Γ and therefore increasing the efficiency of solving for ϕ . We detail this forgetting method below, labeled “unprincipled” because the decision about which entries in v to forget is made in an *ad hoc* manner.

Consider following the process as described in Section III A to solve for a random $N = 2$ trajectory up through $T - 1$ time steps, then seeking to randomly generate the potential value at ϕ_T . For simplicity, we only consider values of V and not its derivatives in this trajectory. The constraining power of Γ is quantified by the sum of the eigenvalues (i.e., the trace) of Γ_C : *higher* values of $\text{Tr}(\Gamma_C)$ correspond to *looser* constraints (higher variance in generated points). Consider removing rows/columns of Γ corresponding to early data, V_i, V_1, V_2 etc., one at a time and recomputing some $\tilde{\Gamma}_C$ after each removal. In Figure 5, it is shown that the number of rows kept in Γ as a fraction of T can be as low as ~ 0.5 before $\text{Tr}(\tilde{\Gamma}_C)$ changes by more than 10% of itself.

To jointly quantify the amount of time saved and the resultant accuracy of the unprincipled forgetting method, we ran 50 simulations with the `bushwhack` code, param-

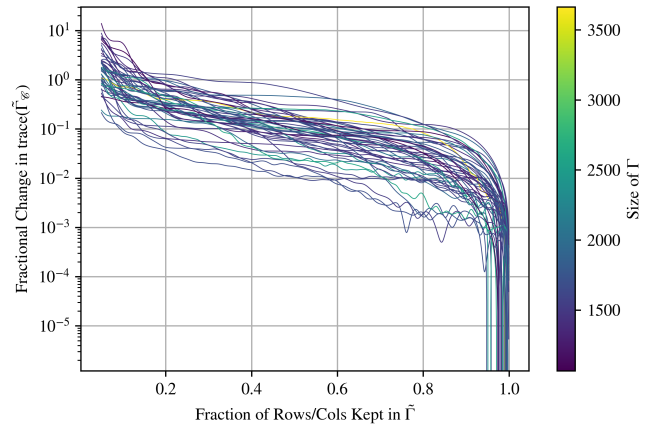


FIG. 5. Constraining power lost from the covariance matrix Γ as a function of kept information. As more information is removed from earlier in the simulation (lower values on the horizontal axis), the constraints on a new potential value become more relaxed (the trace of the conditional covariance matrix $\tilde{\Gamma}_C$ increases). However, the constraining power of Γ is retained even with many rows and columns removed.

eters $(s, V_*, N, \phi_i) = (30, 5 \cdot 10^{-9}, 2, 0.8s)$, without any compression methods. For each run, we saved the total simulation time t_{sim} , predicted value for A_S , and random state, then reran the simulation (with the same random state) 5 times, each executing unprincipled forgetting steps once Γ reached some variable maximum size. For each rerun we, again, stored the compressed simulation time \tilde{t}_{sim} and compressed prediction for the matter spectral amplitude \tilde{A}_S . The left panel of Figure 6 demonstrates that the fractional time taken $\tilde{t}_{\text{sim}}/t_{\text{sim}}$ decreases as a power law with t_{sim} . The time saved can achieve values of 1/5 with conservative compression and 1/50 with high compression while simultaneously predicting \tilde{A}_S to be very nearly correct. The right panel of Figure 6 confirms that higher degrees of compression tend to produce less accurate predictions, but assures that these inaccuracies are small enough at moderately high levels. Given the speed-up, accuracy, and ease of implementation of unprincipled forgetting steps, we incorporate them permanently into the `bushwhack` code to execute at a maximum Γ size of 1000^2 .

2. “Principled” Forgetting

In the previous subsection, we described a method for increasing computational efficiency that involved compressing Γ under the assumption that earlier points weakly constrain newly generated data. This method was labeled “unprincipled” because it involved the *ad hoc* (but reasonable) choice to delete points based on their distance from the point of interest. In this section, we describe a “principled” method of compressing Γ that allows for direct control over the portion of trace kept.

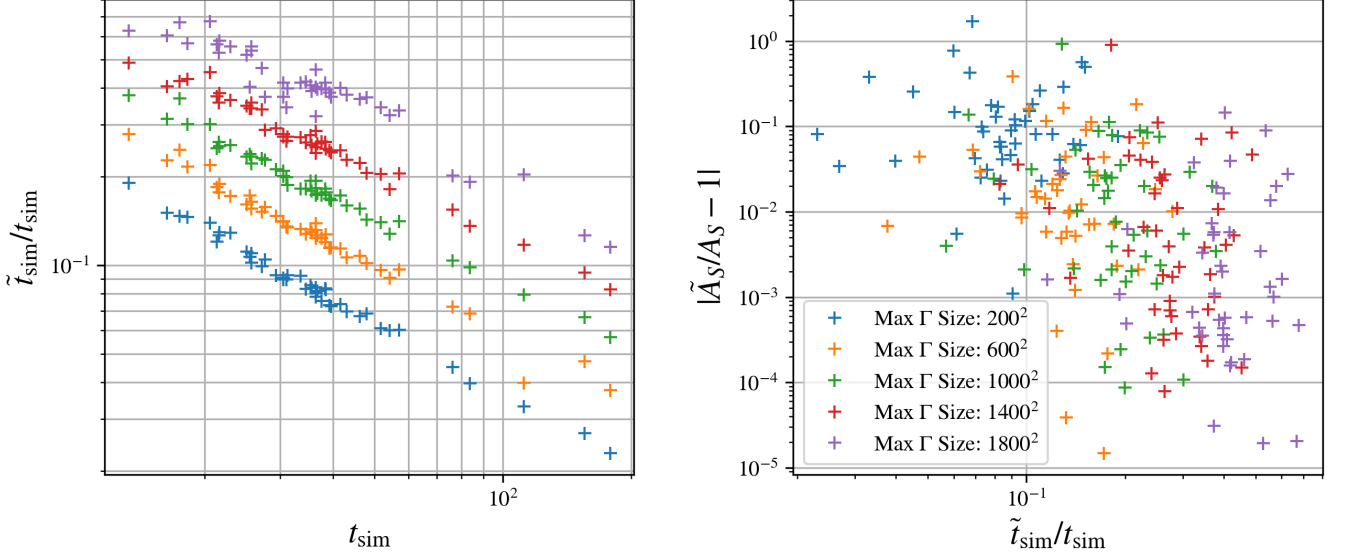


FIG. 6. Quantifying compression and accuracy of “unprincipled” forgetting. *Left:* A simulation without compression steps that takes a time t_{sim} [seconds] to complete can finish in a fraction of the time after incorporating forgetting steps. That fraction $\tilde{t}_{\text{sim}}/t_{\text{sim}}$ falls as a power law with t_{sim} . Colors represent the maximum allowed size of Γ before a compression step is executed: lower maximum size means higher (more frequent) compression. *Right:* Even with high compression, simulations accurately reproduce uncompressed predictions. While higher compression is, indeed, less accurate, a moderate (and helpful) level of compression can be achieved while sustaining reasonably small error.

We leave its implementation in random field inflationary trajectories to future work (see Section V A).

We seek to compress Γ so as to maximize its constraining power while minimizing its overall size. When $\mathbf{v}_{\mathcal{O}}$ gets large, we seek to find a compression matrix \mathbf{A} such that

$$\tilde{\mathbf{v}}_{\mathcal{O}} = \mathbf{A}\mathbf{v}_{\mathcal{O}}, \quad (3.2)$$

where $\tilde{\mathbf{v}}_{\mathcal{O}}$ is a smaller, compressed version of $\mathbf{v}_{\mathcal{O}}$. We can transform blocks of Γ into compressed forms as

$$\tilde{\Gamma}_{\mathcal{O}\mathcal{O}} = \langle \tilde{\mathbf{v}}_{\mathcal{O}} \tilde{\mathbf{v}}_{\mathcal{O}}^T \rangle = \mathbf{A} \Gamma_{\mathcal{O}\mathcal{O}} \mathbf{A}^T \quad (3.3)$$

$$\tilde{\Gamma}_{\mathcal{N}\mathcal{O}} = \langle \tilde{\mathbf{v}}_{\mathcal{N}} \tilde{\mathbf{v}}_{\mathcal{O}}^T \rangle = \Gamma_{\mathcal{N}\mathcal{O}} \mathbf{A}^T \quad (3.4)$$

$$\tilde{\Gamma}_{\mathcal{C}} = \Gamma_{\mathcal{N}\mathcal{N}} - \tilde{\Gamma}_{\mathcal{N}\mathcal{O}} \tilde{\Gamma}_{\mathcal{O}\mathcal{O}}^{-1} \tilde{\Gamma}_{\mathcal{O}\mathcal{N}}. \quad (3.5)$$

As mentioned previously, *lower* values of $\text{Tr}(\tilde{\Gamma}_{\mathcal{C}})$ correspond with *tighter* constraints on new potential generation. Thus, to maximize the constraining power of $\tilde{\Gamma}$, we need to reduce $\text{Tr}(\tilde{\Gamma}_{\mathcal{C}})$ by maximizing the trace of its latter term,

$$\tau \equiv \text{Tr}(\tilde{\Gamma}_{\mathcal{N}\mathcal{O}} \tilde{\Gamma}_{\mathcal{O}\mathcal{O}}^{-1} \tilde{\Gamma}_{\mathcal{O}\mathcal{N}}) \quad (3.6)$$

$$= \text{Tr}(\Gamma_{\mathcal{N}\mathcal{O}} \mathbf{A}^T (\mathbf{A} \Gamma_{\mathcal{O}\mathcal{O}} \mathbf{A}^T)^{-1} \mathbf{A} \Gamma_{\mathcal{O}\mathcal{N}}) \quad (3.7)$$

It is straightforward to show that τ only depends on the row space of \mathbf{A} , so we are free to impose the additional constraint that the rows of \mathbf{A} be orthonormal with respect to $\Gamma_{\mathcal{O}\mathcal{O}}$.

$$\mathbf{A} \Gamma_{\mathcal{O}\mathcal{O}} \mathbf{A}^T = \mathbf{1} \quad (3.8)$$

This constrained maximization problem leads to

$$\mathbf{A} \Gamma_{\mathcal{N}\mathcal{O}} \Gamma_{\mathcal{O}\mathcal{N}} = \boldsymbol{\Lambda} \mathbf{A} \Gamma_{\mathcal{O}\mathcal{O}} \quad (3.9)$$

where $\boldsymbol{\Lambda}$ is a matrix of Lagrange multipliers. We can once again take linear combinations of the rows of \mathbf{A} to diagonalize $\boldsymbol{\Lambda}$. Now, each row \mathbf{a} of \mathbf{A} is a solution to the generalized eigenvalue problem

$$\Gamma_{\mathcal{N}\mathcal{O}} \Gamma_{\mathcal{O}\mathcal{N}} \mathbf{a} = \lambda \Gamma_{\mathcal{O}\mathcal{O}} \mathbf{a}. \quad (3.10)$$

Since $\tau = \sum_i \lambda_i$, the optimal compression matrix will comprise some number of rows corresponding to the largest eigenvalues so that the size of $\tilde{\Gamma}_{\mathcal{O}\mathcal{O}}$ is much less than $\Gamma_{\mathcal{O}\mathcal{O}}$ and $\tau \approx \text{Tr}(\Gamma_{\mathcal{N}\mathcal{O}} \Gamma_{\mathcal{O}\mathcal{O}}^{-1} \Gamma_{\mathcal{O}\mathcal{N}})$. Significant compression may be possible with this method, as the density of data points required to resolve the path evolution of ϕ is often greater than what is necessary to describe the potential in a local domain. An overdensity of data points leads to many redundant constraints on new potential generation, and thus a high concentration of τ in the very largest eigenvalues. We leave proper implementation of principled forgetting to future work.

IV. RESULTS

The `bushwhack` code (see Section III A) was parallelized and implemented with unprincipled forgetting (see Section III B 1) for execution on the University of Richmond Quark Supercomputing Cluster. As a preliminary

Spectral Quantity	μ_q ($N = 1$)	σ_q ($N = 1$)	Tension ($N = 1$)	μ_q ($N = 2$)	σ_q ($N = 2$)	Tension ($N = 2$)	μ_q ($N = 3$)	σ_q ($N = 3$)	Tension ($N = 3$)
$\log_{10}(A_S)$	-9.459	0.060	13.0σ	-9.474	0.055	14.4σ	-9.463	0.368	2.1σ
n_S	0.9636	0.0020	0.5σ	0.9613	0.0020	0.7σ	0.9579	0.0367	0.1σ
$\log_{10}(A_T)$	-10.393	0.101	N/A	-10.431	0.067	N/A	-10.430	0.402	N/A
n_T	-0.0159	0.0021	N/A	-0.0170	0.0010	N/A	-0.0180	0.0009	N/A
$\log_{10}(r)$	-0.906	0.065	1.4σ	-0.928	0.055	1.3σ	-0.939	0.058	1.0σ

TABLE II. Tabulated results and comparisons. Shown are the weighted means, standard deviations, and tensions with Planck data of various spectral quantities for each parameter set (4.1)-(4.3). While A_S predictions exhibit significant tension with Planck data, slight variations in s and/or V_* may be expected to preserve the agreements seen in n_S and r while remedying differences in A_S .

investigation, we choose a some reasonable parameter sets for the generation of V .

$$(s, V_*^2, N) = (30, 5 \cdot 10^{-9}, 1) \quad (4.1)$$

$$(s, V_*^2, N) = (30, 5 \cdot 10^{-9}, 2) \quad (4.2)$$

$$(s, V_*^2, N) = (30, 5 \cdot 10^{-9}, 3) \quad (4.3)$$

The only variable between these sets is N , which may change predictions of observable quantities in nontrivial ways, though varying s and V_* is worthwhile future work.

To gather a representative sample of trajectories from a given parameter set, we catalogue 1000 simulations with ϕ_i chosen from each of 12 radial ϕ -shells of thickness $0.1s$ from $0.3s$ to $2.1s$. That is, we randomly choose the initial distance from the minimum at the origin to lie within a certain bin (for instance, $\phi_i \in [0.8s, 0.9s]$), then randomly choose the vector location ϕ_i , all 1000 times in each bin. If $\phi_i < 0.3s$, the trajectory is very unlikely to accumulate

enough inflation, and if $\phi_i > 2.1s$, exponentially unlikely to converge to the origin.

A. Weighting Predictions by Success Probabilities

The probability P_S that a trajectory succeed – converges to the origin with enough inflation – is an interesting function of ϕ_i , plotted at each discrete shell for our chosen parameter sets in Figure 7. To correctly compute the statistical predictions of parameter sets from individual trajectories, it is necessary to weight runs by this function $P_S(\phi_i)$, since there is not an equal likelihood that each trajectory could have naturally occurred. For instance, a successful trajectory with $\phi_i = 2s$ is very unlikely, so its predicted value for r should be a minute contribution to the weighted mean relative to much more commonly successful runs.

In a given parameter set, for some predicted observable quantity q , the weighted mean μ_q considers all shells l as

$$\mu_q = \frac{\sum_l w_l q_l}{\sum_l w_l} \quad (4.4)$$

where $w_l = P_S(l)$ is a shell weight and q_l is the simple mean of q within l . Similarly, the variance of q is

$$\sigma_q^2 = \frac{\sum_l w_l q_l^2}{\sum_l w_l} - \mu_q^2. \quad (4.5)$$

B. Power Spectra Predictions

We now present the statistical predictions for observable quantities computed from a Gaussian random inflaton potential with parameters sets (4.1)-(4.3). We assume any error resulting from compression methods is accurately represented in the variance of the outputted spectral quantities. First, we examine Figure 8, which shows weighted, normalized histograms for each of A_S, n_S, A_T, n_T , and r for each parameter set, colored by initial condition. A few observations to note:

- Changing N does not significantly affect the mean or variance of any quantity. Future work into

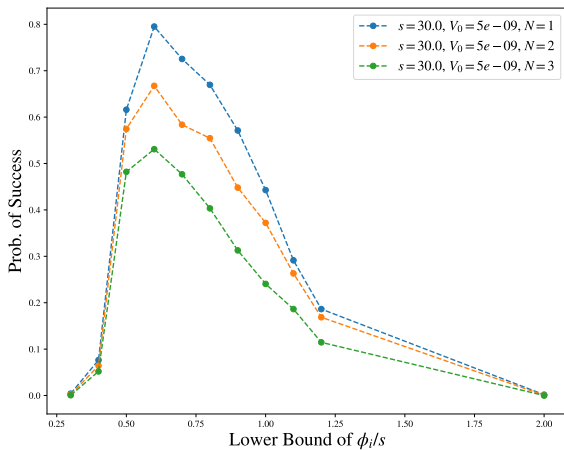


FIG. 7. The probability that a trajectory starting at an initial distance ϕ_i from the origin will both converge and accumulate enough inflation. We did not simulate in the shells between $1.4s$ and $2.0s$ to save time, since the behavior would be well documented by a single data point at $2.0s$.

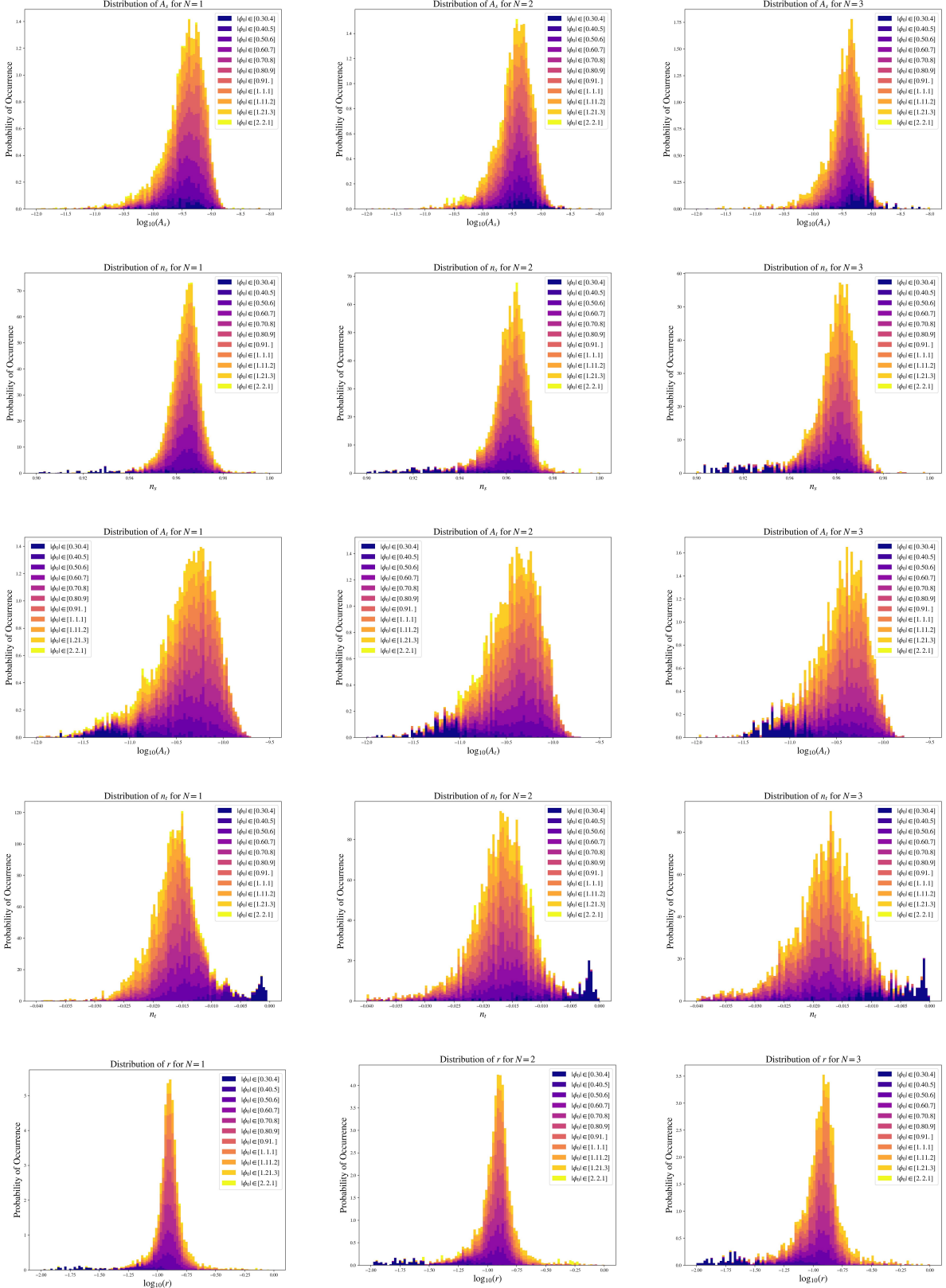


FIG. 8. Weighted histograms of observable quantities A_S , n_S , A_T , n_T , and r . Different colors on each histogram correspond to different initial positions ϕ_i . Each row of plots corresponds to a particular spectral quantity and each column to a parameter set. Horizontal axes are the same along each row.

higher N is required to confirm that these quantities are insensitive to the dimension of V .

- Quantity distributions within ϕ_i shells are not necessarily the same as the weighted distributions over entire parameter sets. This is especially apparent in the low ϕ_i regime (darker blues); secondary peaks are observed in distributions of A_T and n_T (and, by proxy, r) that are almost completely void of predictions from high ϕ_i simulations.
- Predicted mean values are in variable tension with Planck observations, detailed in Table II. For example, A_S is lower than the Planck prediction for all $N = 1, 2, 3$, while n_S predictions are tightly distributed around the accepted value. Note that this does not indicate that the Gaussian random potential cannot accommodate all Planck predictions, but that the particular parameter sets (4.1)-(4.3) are not the best fit.
- Distributions roughly normal, but some (in particular n_S and A_T) have slight negative skewness. Thus, the variance may not be the best metric of statistical spread for each quantity.

The predictions visualized in each histogram are quantified in Table II. We also present some spectral quantities plotted against each other as scatterplots (colored, again, by ϕ_i) and Gaussian kernel density estimations (KDEs) in Figure 9. These panels further emphasize a few points:

- The scatterplots do not incorporate weights into their visuals, so the lack of resemblance to a multivariate normal distribution is apparent. However, the appropriately weighted KDEs still exhibit curving, non-trivial relationships between quantities.
- The starting location ϕ_i is a highly relevant initial condition for trajectories in Gaussian random potentials. Different ϕ_i bins predict quantities clustered in different regions of the scatterplots. Deep blues (low ϕ_i) and bright yellows (high ϕ_i) show interesting differences from the bulk of the distribution and, even though they are de-weighted to near-negligible contributions, may become of interest with anthropic principle arguments.
- While a majority of the weight goes to tighter regions (as seen in the KDEs), the Gaussian random potential admits many dramatic outliers, making the model all the more interesting and adaptable to modern constraints.

In total, there are ten different combinations of quantities for each of $N = 1, 2, 3$ that could be shown as rows in Figure 9, but the chosen three are especially demonstrative and enlightening.

V. CONCLUSIONS

We have presented a method for exploration into N -dimensional inflationary models in which the inflaton potential is realized via a Gaussian random process. Information about the potential is not computed throughout a volume, but efficiently generated along the path evolution of the inflaton field. Even still, the covariance matrix of constraints Γ can grow large and unwieldy, as it must track N first derivatives and N^2 second derivatives at each time step for complete precision. We propose two methods of compression, “unprincipled” and “principled” forgetting, that may help to ease the computational intensity by exploiting weak or redundant constraints within Γ . We implement unprincipled forgetting steps into our differential equations solver and compile thousands of simulations to characterize the predictions of Gaussian random potentials with three particular parameter sets. We list our main conclusions below:

- The Gaussian random potential is a highly versatile inflationary model with a rich volume of promising parameter space. Parameters s , V_* , N , and ϕ_i each change the statistical predictions for perturbation spectra in unique ways. Some parameter sets (such as (4.1)-(4.3)) have been demonstrated to accurately predict a number of spectral quantities in Figures 8 and 9.
- Algorithmic data compression allows for the possibility of significantly more efficient generation of V in high- N regimes. Unprincipled forgetting is limited in that it relies on the assumption that earlier data contributes weaker constraints on new generation and less rigorous in that it involves the deletion of data rather than compression. Principled forgetting methods, if implemented efficiently, could remedy these issues.

A. Future Work

This project could be further explored in a number of ways, ranked below by priority.

1. *Explore parameter space.* Carry out a large number of simulations with different parameter sets which vary s and V_* in addition to N . These supplemental runs could quantify the degree to which the Gaussian random potential model is able to accurately reproduce modern constraints on primordial power spectra.
2. *Implement principled forgetting.* Unprincipled forgetting offers significant speed increases, but at the expense of rigorous algorithmic data compression. Principled forgetting methods detailed in Section III B 2 have the capacity to provide enormous compression to Γ , possibly enough to efficiently explore string-theory-esque models with $N \sim 100$.

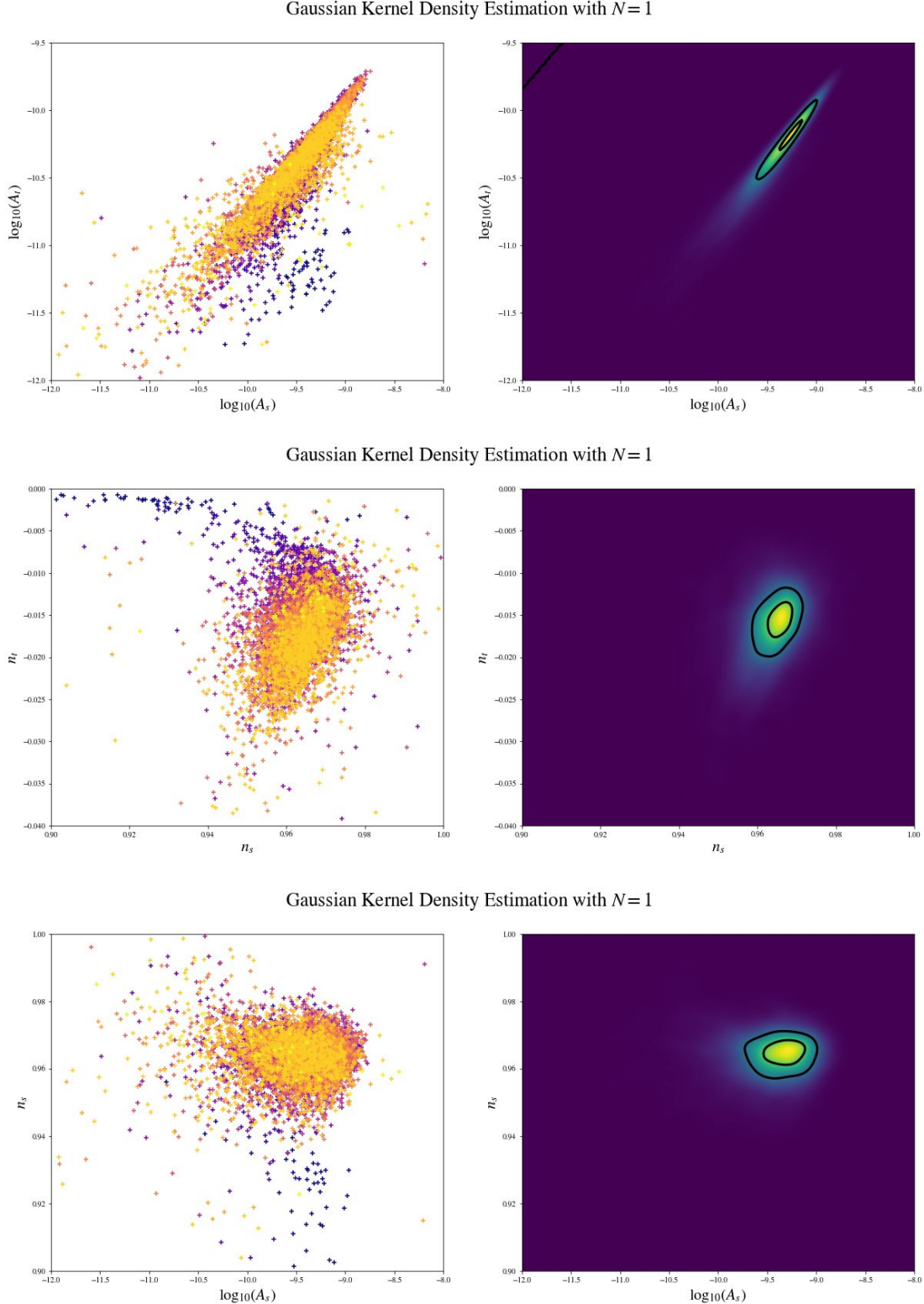


FIG. 9. Gaussian kernel density estimations (KDEs) of scatter-plotted predictions for perturbation spectra. Each cross on the scatter plots corresponds to the prediction of one individual trajectory. The colors of crosses are identical to those in Figure 8. About 11000 individual points are plotted, but many are obscured by points plotted later. The KDEs express the density of the points on the scatter plot. The closed black curves indicate the areas enclosing 68% (inner) and 95% (outer) of the weighted distribution of data. Note that the scatter plots do not incorporate the weighting described in Section IV A, but the KDEs do.

3. *Incorporate other observables.* The spectral quantities computed from our trajectories are but a subset of the independent quantities constrained by modern observations. Incorporating quantities such as the non-Gaussianity of the CMB could further verify whether the Gaussian random potential is a plausible inflationary model of our universe [30].
4. *Translate to other languages.* The **bushwhack** code is currently written in Python, but could be optimized by translating to more efficient languages such as C or FORTRAN.

ACKNOWLEDGEMENTS

This project was supported by two Summer Research Fellowships from the University of Richmond School of Arts & Sciences from May 2019 to July 2020. Simulations were run on the University of Richmond Quark Supercomputing Cluster, purchased with a Major Research Instrumentation grant from the National Science Foundation. EFB thanks Andrew Jaffe and Alan Heavens for enlightening conversations and Imperial College for its hospitality during the beginning of this work.

-
- [1] S. Dodelson, *Modern Cosmology*, 1st ed. (Academic Press, 2003).
- [2] D. Langlois, Inflation and cosmological perturbations, Lecture Notes in Physics , 1–57 (2010).
- [3] D. S. Salopek, J. R. Bond, and J. M. Bardeen, Designing density fluctuation spectra in inflation, Phys. Rev. D **40**, 1753 (1989).
- [4] D. Baumann and L. McAllister, *Inflation and String Theory* (Cambridge University Press, 2015).
- [5] A. Aazami and R. Easther, Cosmology from random multifield potentials, J. Cosmol. Astropart. Phys **2006**, 013 (2006), arXiv:hep-th/0512050 [hep-th].
- [6] M. C. D. Marsh, L. McAllister, E. Pajer, and T. Wrane, Charting an Inflationary Landscape with Random Matrix Theory, J. Cosmol. Astropart. Phys **2013**, 040 (2013), arXiv:1307.3559 [hep-th].
- [7] M. Dias, J. Frazer, and M. C. D. Marsh, Simple Emergent Power Spectra from Complex Inflationary Physics, Phys. Rev. Lett. **117**, 141303 (2016), arXiv:1604.05970 [astro-ph.CO].
- [8] M. Dias, J. Frazer, and M. C. D. Marsh, Seven lessons from manyfield inflation in random potentials, J. Cosmol. Astropart. Phys **2018**, 036 (2018), arXiv:1706.03774 [astro-ph.CO].
- [9] M. Yamada and A. Vilenkin, Hessian eigenvalue distribution in a random Gaussian landscape, Journal of High Energy Physics **2018**, 29 (2018), arXiv:1712.01282 [hep-th].
- [10] S. Paban and R. Rosati, Inflation in multi-field modified DBM potentials, J. Cosmol. Astropart. Phys **2018**, 042 (2018), arXiv:1807.07654 [astro-ph.CO].
- [11] L. Lerh Feng, S. Hotchkiss, and R. Easther, The distribution of vacua in random landscape potentials, J. Cosmol. Astropart. Phys **2021**, 029 (2021), arXiv:2004.04429 [hep-th].
- [12] B. Freivogel, R. Gobetti, E. Pajer, and I.-S. Yang, Inflation on a Slippery Slope, arXiv e-prints , arXiv:1608.00041 (2016), arXiv:1608.00041 [hep-th].
- [13] G. Wang and T. Battefeld, Random functions via Dyson Brownian Motion: progress and problems, J. Cosmol. Astropart. Phys **2016**, 008 (2016), arXiv:1607.02514 [hep-th].
- [14] R. Easther, A. H. Guth, and A. Masoumi, Counting Vacua in Random Landscapes, arXiv e-prints , arXiv:1612.05224 (2016), arXiv:1612.05224 [hep-th].
- [15] A. Masoumi, A. Vilenkin, and M. Yamada, Initial conditions for slow-roll inflation in a random Gaussian landscape, J. Cosmol. Astropart. Phys **2017**, 003 (2017), arXiv:1704.06994 [hep-th].
- [16] T. Bjorkmo and M. C. D. Marsh, Manyfield inflation in random potentials, J. Cosmol. Astropart. Phys **2018**, 037 (2018), arXiv:1709.10076 [astro-ph.CO].
- [17] T. Battefeld and C. Modi, Local random potentials of high differentiability to model the Landscape, J. Cosmol. Astropart. Phys **2015**, 010 (2015), arXiv:1409.5135 [hep-th].
- [18] S.-H. H. Tye, J. Xu, and Y. Zhang, Multi-field inflation with a random potential, Journal of Cosmology and Astroparticle Physics **2009** (04), 018–018.
- [19] L. C. Price, H. V. Peiris, J. Frazer, and R. Easther, Designing and testing inflationary models with bayesian networks, Journal of Cosmology and Astroparticle Physics **2016** (02), 049.
- [20] T. Rudelius, Learning to inflate. A gradient ascent approach to random inflation, J. Cosmol. Astropart. Phys **2019**, 044 (2019), arXiv:1810.05159 [hep-th].
- [21] J. J. Blanco-Pillado, K. Sousa, and M. A. Urkola, Slepian models for Gaussian random landscapes, Journal of High Energy Physics **2020**, 142 (2020), arXiv:1911.07618 [hep-th].
- [22] L. C. Price, J. Frazer, J. Xu, H. V. Peiris, and R. Easther, Multimodecode: an efficient numerical solver for multi-field inflation, Journal of Cosmology and Astroparticle Physics **2015** (03), 005–005.
- [23] Y. Akrami, F. Arroja, M. Ashdown, J. Aumont, C. Bacigalupi, M. Ballardini, A. J. Banday, R. B. Barreiro, N. Bartolo, and et al., Planck2018 results, Astronomy & Astrophysics **641**, A10 (2020).
- [24] W. H. Press, S. A. Teukolsky, W. T. Vetterling, and B. P. Flannery, *Numerical Recipes 3rd Edition: The Art of Scientific Computing*, 3rd ed. (Cambridge University Press, USA, 2007).
- [25] Y. Hoffman and E. Ribak, Constrained Realizations of Gaussian Fields: A Simple Algorithm, Astrophys. J. Lett. **380**, L5 (1991).
- [26] G. B. Rybicki and W. H. Press, Interpolation, Realization, and Reconstruction of Noisy, Irregularly Sampled Data, Astrophys. J. **398**, 169 (1992).
- [27] J. D. Barrow and F. J. Tipler, *The anthropic cosmological principle*. (Oxford University Press, 1988).
- [28] G. Efstathiou, An anthropic argument for a cosmological constant, M.N.R.A.S. **274**, L73 (1995).
- [29] L. Susskind, The anthropic landscape of string theory, in *Universe or Multiverse?*, edited by B. Carr (Cambridge

University Press, 2007) p. 247.

- [30] S. Renaux-Petel, Combined local and equilateral non-gaussianities from multifield dbi inflation, *Journal of Cosmology and Astroparticle Physics* **2009** (10), 012–012.